Simultaneous control of quantum phase synchronization and entanglement dynamics in a gain-loss optomechanical cavity system

Joy Ghosh,[1,*] Souvik Mondal,[2] Shailendra K. Varshney,[2,1] and Kapil Debnath[2,3,†]

[1]*School of Nanoscience and Technology, IIT Kharagpur, West Bengal 721302, India*

[2]*Electronics and Electrical Communication Engineering Department, IIT Kharagpur, West Bengal 721302, India*

[3]*School of Natural and Computing Sciences, University of Aberdeen, Aberdeen AB24 3UE, Scotland, United Kingdom*

(Received 13 September 2023; accepted 19 January 2024; published 12 February 2024)

The optomechanical cavity system has been a paradigm in the manifestation of continuous variable quantum information over the past decade. This paper investigates how quantum phase synchronization is associated with bipartite Gaussian entanglement in coupled gain-loss mechanical oscillators, where the gain and loss rates can be controlled by driving the cavities with blue and red detuned lasers, respectively. We examine the role of the exceptional point (EP) in a deterministic way of producing self-sustained oscillations that generate robust quantum correlations among quadrature fluctuations of the mechanical oscillators. Particularly, steady phase synchronization dynamics along with the entanglement phenomena are observed in the effective weak-coupling regime above a critical driving power. These phenomena are further verified by observing the mechanical squeezing and phase-space rotations of the Wigner distributions. Moreover, the fidelity fluctuation shows how the quantum correlation dynamics are related to the EP of the system. We also discuss the impact of the mechanical oscillator's frequency mismatch and decoherence due to thermal phonons on system dynamics. These findings hold promise for applications in phonon-based quantum communication and information processing on the macroscopic scale.

DOI: 10.1103/PhysRevA.109.023512

I. INTRODUCTION

Synchronization is a natural phenomenon widely observed around us, where two or more systems tend to act similarly at the same time. During the early 17th century, Huygens first proposed that mechanical clocks hanging from a common support tend to oscillate in unison by overcoming their natural frequency disorder [1]. Since then, it has been found in various processes such as the flashing of fireflies, chemical reactions, neuron networks, and heart cells [2]. Synchronization in different classical setups was extensively studied in the past, but in the quantum limit, it gained popularity after Mari *et al.* proposed a measure to compute complete synchronization and phase synchronization for continuous variable systems [3]. This has been applied in various systems like cavity quantum electrodynamics [4], atomic ensembles [5], van der Pol oscillators [6], and spin chains [7]. The study of synchronization among classical oscillators is usually modeled in the framework of nonlinear dynamics, where limit cycle solutions exist and the oscillators tend to synchronize due to the mutual interaction in a steady state. However, the principle of quantum synchronization differs fundamentally from its classical counterpart due to Heisenberg's uncertainty relation [3]. It is well known that synchronization is closely linked to other quantum correlations, such as entanglement [7], mutual information [8], and geometric discord [9]. Particularly, the coexistence of quantum synchronization and entanglement is a captivating phenomenon. Earlier studies have demonstrated that superconducting qubits that emit entangled photons can be synchronized [10]. Also, clock synchronization is achieved using entangled photons generated by parametric down-conversion [11], and in quantum many-body systems, entanglement and synchronization lead to collective cooperative behavior [12]. Moreover, spin-1 systems can also be synchronized through entanglement [7].

In this context, optomechanical architectures [13] appeared to be a promising platform to test synchronization and entanglement among micro- or nanomechanical oscillators, where two mechanical or cavity modes can be directly coupled through phonon or photon hopping. Multiple synchronization schemes have been developed in optomechanics [14–17], among which enhancing the nonlinearity is considered a primary feature, for which periodic modulation, quadratic coupling, and optical parametric amplifiers are frequently used [18–21]. The curiosity about the interplay between quantum synchronization and entanglement in optomechanical setup is emerging in recent times [21–24]. Previously it has been demonstrated through optical coupling only, and the mechanical interaction-based design is still unexplored. The idea of exceptional points (EPs) [25] in coupled gain-loss structures is a novel tool that can be applied for this purpose. EPs refer to fundamental degeneracies in gain-loss cavities or waveguides [26–28], where the system's eigenvalues coalesce and become degenerate. EP-based optomechanical structures have been studied for mass sensing [29], optomechanically induced transparency [30], and sideband generation [31]

*joyghos@kgpian.iitkgp.ac.in

†kapil.debnath@abdn.ac.uk

offering better controllability for operation. Synchronization and frequency locking in the classical domain [32–34] and entanglement generation in $\mathcal{PT}$ symmetric structures [35–37] are also proposed via EP engineering. However, promising advantages of EPs need further exploration to feature intriguing quantum correlation properties in different systems.

Here, we present a configuration consisting of two mechanically coupled gain-loss optomechanical cavities (OMCs) by controlling the laser detuning. This configuration leads to self-sustained oscillations through EP in a deterministic way [31], which is essential for investigating quantum phase synchronization and entanglement between the two oscillators. Based on the numerical calculations, a rich connection between quantum synchronization and entanglement is further clarified. It is noteworthy to mention that no entanglement was observed in the mechanically coupled system despite achieving synchronization in Ref. [3]. In this paper, we present the EP-induced limit cycles to obtain various dynamics of quantum phase synchronization and entanglement simultaneously. Also, in contrast to the earlier attempts at demonstrating entanglement through coupling coefficient variation [35,36], the driving field strength is suitably modified in our analysis to switch the coupling from strong to weak regimes. The exceptional point in this system reveals an intriguing relationship between mechanical squeezing characteristics and fidelity dynamics of the oscillators, which have not been studied so far. The proposed method in this paper allows simultaneous control of the dynamics of quantum phase synchronization and entanglement, which can be applied in quantum communication protocols and information processing schemes.

The paper is organized as follows. In Sec. II, the quantum Langevin equations are derived from the system Hamiltonian. The classical dynamics are analyzed and the stability of the system is presented in the consequent subsections. Next, we present the covariance matrix (CM) approach to quantify quantum phase synchronization and entanglement measurement schemes. Section III presents the important results and discussion about the possible relationship between these two phenomena, and Sec. IV concludes the paper.

II. THEORETICAL MODEL

A. Hamiltonian and quantum Langevin equations

The schematic of the proposed setup is depicted in Fig. 1. It consists of two optomechanical cavities that are identical but oppositely detuned, both coupled mechanically. The coupling between the two oscillators is facilitated through phonon tunneling. By adjusting the laser driving power, one can tune the mechanical coupling between the two oscillators. The Hamiltonian of the complete system can be expressed as follows (taking $\hbar = 1$):

$$\hat{\mathcal{H}} = \sum_{j=1,2}\Big[-\Delta_j\hat{a}_j^\dagger\hat{a}_j + \frac{\omega_{mj}}{2}\big(\hat{p}_j^2+\hat{q}_j^2\big) - g_{0j}\hat{a}_j^\dagger\hat{a}_j\hat{q}_j + iE_j(\hat{a}_j^\dagger - \hat{a}_j)\Big] - J\hat{q}_1\hat{q}_2. \quad (1)$$

The Hamiltonian is written in the rotating frame of the driving frequency (ω_L) with cavity detuning from optical

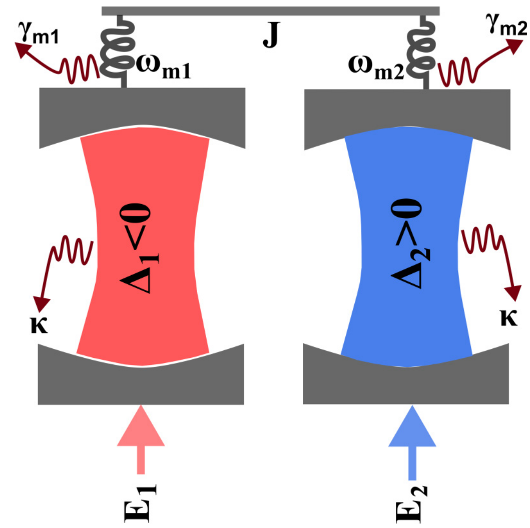

FIG. 1. Schematic diagram of two Fabry-Pérot cavities coupled mechanically with strength J and driven by red ($\Delta_1 < 0$) and blue ($\Delta_2 > 0$) detuned laser fields, respectively. The opposite detunings characterize the gain-loss effect, whereas E_j ($j = 1, 2$) represents the amplitude of optical driving power provided. The natural frequencies of the vibrating oscillators are assumed to be nearly equal, i.e., $\omega_{m1} \approx \omega_{m2}$.

resonance, which is given as $\Delta_j = \omega_L - \omega_{oj}$. Here $\hat{a}_j^\dagger(\hat{a}_j)$ are the creation (annihilation) operators associated with the optical field with frequency ω_{oj}, and $\hat{q}_j$ and $\hat{p}_j$ are the dimensionless position and momentum operators of the jth mechanical oscillators with frequencies ω_{mj}. The optomechanical coupling of each cavity is g_{0j} and the laser driving field strength of the two single-mode cavities is E_j. The last term in the Hamiltonian represents the mechanical interaction, acting as a bosonic Gaussian channel between the oscillators with strength J, assumed to be much smaller than mechanical frequency ($J \ll \omega_{mj}$). The interaction Hamiltonian indicates the potential energy of the mechanically coupled oscillator system, and it depends on the product of displacement operators, showing influences of the oscillator's motion on one another. The dissipative dynamics of the system are described by the following set of nonlinear quantum Langevin equations:

$$\begin{aligned}
\partial_t\hat{a}_j &= -(\kappa - i\Delta_j)\hat{a}_j + ig_0\hat{a}_j\hat{q}_j + E_j + \sqrt{2\kappa}\hat{a}_j^{\text{in}},\\
\partial_t\hat{q}_j &= \omega_{mj}\hat{p}_j,\\
\partial_t\hat{p}_j &= -\omega_{mj}\hat{q}_j - \gamma_{mj}\hat{p}_j + J\hat{q}_{3-j} + g_0\hat{a}_j^\dagger\hat{a}_j + \hat{\eta}_j. \quad (2)
\end{aligned}$$

Here, γ_{mj} and κ represent the intrinsic dissipation of mechanical oscillators and optical cavities, respectively. In analytical formulations, the cavity decay rate (κ) and optomechanical constant (g_{0j}) are assumed identical for both cavities for the sake of simplicity. The laser driving amplitude provided for both cavities is also taken as the same, i.e., $E_1 = E_2 = E$. The stochastic noise operators for optical and mechanical systems are given as $\hat{a}_j^{\text{in}}$ and $\hat{\eta}_j$, satisfying the standard correlation $\langle\hat{a}_i^{\text{in}\dagger}(t)\hat{a}_j^{\text{in}}(t') + \hat{a}_j^{\text{in}\dagger}(t')\hat{a}_i^{\text{in}}(t)\rangle = \delta_{ij}\delta(t-t')$ and $\frac{1}{2}\langle\hat{\eta}_i(t)\hat{\eta}_j(t') + \hat{\eta}_j(t')\hat{\eta}_i(t)\rangle = \gamma_{mj}(2n_m+1)\delta_{ij}\delta(t-t')$ under

Markovian approximation [38,39]. The mean thermal phonon occupancy at temperature T of the mechanical systems for nearly equal operating frequencies is taken as $n_m = [\exp(\frac{\hbar\omega_m}{k_B T}) - 1]^{-1}$ (where k_B is the Boltzmann constant). Assuming a strongly driven cavity field, the quantum Langevin equations are usually solved using the standard linearization technique, where the classical mean dynamics and quadrature fluctuations of the operators are separated, i.e., $\hat{\mathcal{O}}(t) = \langle\hat{\mathcal{O}}(t)\rangle + \delta\hat{\mathcal{O}}(t)$, where $\mathcal{O} = a_j, q_j, p_j$. The classical dynamical equations are given as

$$\begin{aligned}
\partial_t\langle\hat{a}_j\rangle &= -(\kappa - i\Delta_j)\langle\hat{a}_j\rangle + ig_0\langle\hat{q}_j\rangle\langle\hat{a}_j\rangle + E,\\
\partial_t\langle\hat{q}_j\rangle &= \omega_{mj}\langle\hat{p}_j\rangle,\\
\partial_t\langle\hat{p}_j\rangle &= -\omega_{mj}\langle\hat{q}_j\rangle - \gamma_{mj}\langle\hat{p}_j\rangle + J\langle\hat{q}_{3-j}\rangle + g_0|\langle\hat{a}_j\rangle|^2. \quad (3)
\end{aligned}$$

Neglecting higher-order terms, the linearized quantum Langevin equations describing quadrature fluctuations are as follows:

$$\begin{aligned}
\partial_t\delta\hat{a}_j &= -(\kappa - i\Delta_j)\delta\hat{a}_j + ig_0(\langle\hat{a}_j\rangle\delta\hat{q}_j + \langle\hat{q}_j\rangle\delta\hat{a}_j)\\
&\quad + \sqrt{2\kappa}\,\delta\hat{a}_j^{\mathrm{in}},\\
\partial_t\delta\hat{q}_j &= \omega_{mj}\delta\hat{p}_j,\\
\partial_t\delta\hat{p}_j &= -\omega_{mj}\delta\hat{q}_j - \gamma_{mj}\delta\hat{p}_j + J\delta\hat{q}_{3-j} + g_0(\langle\hat{a}_j\rangle\delta\hat{a}_j^\dagger\\
&\quad + \langle\hat{a}_j\rangle^*\delta\hat{a}_j) + \hat{\eta}_j. \quad (4)
\end{aligned}$$

B. Effective coupled mechanical system

The effective coupled mechanical oscillator picture can be found by first introducing the creation and annihilation operators of the mechanical modes defined as $\hat{b}_j = \frac{\hat{q}_j + i\hat{p}_j}{\sqrt{2}}$ and $\hat{b}_j^\dagger = \frac{\hat{q}_j - i\hat{p}_j}{\sqrt{2}}$. Subsequently, the coupled mechanical system discarding noise terms is described by the following classical equations:

$$\begin{aligned}
\partial_t\langle\hat{a}_j\rangle &= -[\kappa - i(\Delta_j + 2g_0\,\mathrm{Re}\langle\hat{b}_j\rangle)]\langle\hat{a}_j\rangle + E,\\
\partial_t\langle\hat{b}_1\rangle &= -(i\omega_{m1} + \gamma_{m1})\langle\hat{b}_1\rangle + iJ\langle\hat{b}_2\rangle + ig_0|\langle\hat{a}_1\rangle|^2,\\
\partial_t\langle\hat{b}_2\rangle &= -(i\omega_{m2} + \gamma_{m2})\langle\hat{b}_2\rangle + iJ\langle\hat{b}_1\rangle + ig_0|\langle\hat{a}_2\rangle|^2. \quad (5)
\end{aligned}$$

Next, we write $\langle\hat{b}_j\rangle$ by using the ansatz formula as $\langle\hat{b}_j\rangle = \beta_j^{\mathrm{SS}} + \tilde{\beta}_j\exp(-i\bar{\omega}_m t)$, where β_j^{SS} denotes the average displacement in the steady state and $\tilde{\beta}_j$ is the slowly varying time-dependent amplitude with locking frequency $\bar{\omega}_m$. By utilizing this ansatz formula, it is easy to eliminate the cavity modes $\langle\hat{a}_j\rangle$ from the system of equations Eq. (5) [32] (detailed analysis is presented in Appendix). The resulting coupled mechanical modes can be described by the effective Hamiltonian dynamics as $i\partial_t\Psi = \mathcal{H}_{\mathrm{eff}}\Psi$, with the eigenvector $\Psi = [\langle\hat{b}_1\rangle \quad \langle\hat{b}_2\rangle]^T$ and the effective Hamiltonian matrix

$$\mathcal{H}_{\mathrm{eff}} = \begin{pmatrix} \omega_{\mathrm{eff}}^1 - i\gamma_{\mathrm{eff}}^1 & -J \\ -J & \omega_{\mathrm{eff}}^2 + i\gamma_{\mathrm{eff}}^2 \end{pmatrix}. \quad (6)$$

Here ω_{eff}^j and γ_{eff}^j are optomechanically modified mechanical frequencies and damping rates, respectively, due to the elimination of cavity modes. The effective frequency modification is negligible in the resolved sideband setup and thus can be safely neglected [31]. The effective decay and gain rate modifications are expressed as $\gamma_{\mathrm{eff}}^1 = \gamma_{\mathrm{opt}}^1 + \gamma_{m1}$ and $\gamma_{\mathrm{eff}}^2 = \gamma_{\mathrm{opt}}^2 - \gamma_{m2}$ [40], where $\gamma_{\mathrm{opt}}^j \approx \frac{4g_0^2}{\kappa}|\langle\hat{a}_j\rangle^{\mathrm{SS}}|^2$ [41] is the amount of optomechanical inclusion in the mechanical oscillators damping rates. The eigenfrequencies of the effective Hamiltonian are found as

$$\epsilon^{\pm} \approx \frac{\omega_{m1} + \omega_{m2}}{2} - i\frac{\gamma_{\mathrm{eff}}^1 - \gamma_{\mathrm{eff}}^2}{4} \pm \Lambda \quad (7)$$

with $\Lambda = \sqrt{J^2 - (\frac{\gamma_{\mathrm{eff}}^1 + \gamma_{\mathrm{eff}}^2}{4})^2}$. This non-Hermitian system has eigenvalues of the form $\epsilon^{\pm} = \omega^{\pm} + i\gamma^{\pm}$ where real and imaginary parts of the eigenspectrum denote the mechanical frequencies and damping of the system. From Eq. (7) it can be seen that the phase transition between strongly coupled and weakly coupled regimes in parameter space occurs at $J_c = (\gamma_{\mathrm{eff}}^1 + \gamma_{\mathrm{eff}}^2)/4$, which is also known as the exceptional point. The effective strong coupling exhibits for $J > (\gamma_{\mathrm{eff}}^1 + \gamma_{\mathrm{eff}}^2)/4$, while $J < (\gamma_{\mathrm{eff}}^1 + \gamma_{\mathrm{eff}}^2)/4$ stands for the effective weak-coupling regime. The two transition regimes merge at the EP, which can be determined by adjusting either the effective damping rates (γ_{eff}^j) or the mechanical coupling strength (J).

C. Classical dynamics

To determine various temporal dynamics of the mechanical oscillators and identify the phase transition via exceptional points, the set of Eq. (3) is numerically solved by setting initial conditions to zero. In this analysis, we fixed the mechanical coupling strength at $J = 3 \times 10^{-2}\omega_m$ and varied the effective damping rates γ_{eff}^j by changing the optical driving amplitude E. As the same laser driving is incident in both cavities, we can safely choose $\gamma_{\mathrm{opt}}^1 \approx \gamma_{\mathrm{opt}}^2$. The intrinsic damping rate of the loss oscillator is taken to be higher than the gain oscillator, i.e., $\gamma_{m1} = 10^{-2}\omega_m$ and $\gamma_{m2} = 10^{-4}\omega_m$, which has implications regarding the system stability, and a detailed discussion is provided later. The optomechanical coupling constant is set at $g_0 = 10^{-4}\omega_m$ and the cavity decay rate is set at $\kappa = 0.1\omega_m$ for both systems. The operating frequencies for the mechanical oscillators are taken as degenerative with small frequency mismatch, given by $\omega_{m1} = \omega_m$ and $\omega_{m2} = 1.008\omega_m$. Here we keep the first cavity red detuned and the second cavity blue detuned, i.e., $-\Delta_1 = \Delta_2 = \omega_m$, which induces the loss and gain effect in the mechanical oscillators. The simulation parameters are taken according to the experiments done in the resolved sideband regime [42]. The critical driving strength for which the phase transition occurs is found using the relation $J_c = \frac{\gamma_{\mathrm{eff}}^1 + \gamma_{\mathrm{eff}}^2}{4}$, in which γ_{eff}^j is related to laser driving amplitude E by Eq. (3). Based on the analytical calculation, the EP occurs in the parameter space of this system at $E = E_p \approx 380\omega_m$ and it resembles closely the numerical simulations performed on the classical dynamical Eq. (3). From Fig. 2 different temporal dynamics of the coupled mechanical system can be observed by varying the driving amplitude over a wide range. The effective strong-coupling condition $J > (\gamma_{\mathrm{eff}}^1 + \gamma_{\mathrm{eff}}^2)/4 = 0.0203\omega_m$ corresponds to the low driving $E < E_p$, represented by Fig. 2(a). Here, strong coupling results in a coherent exchange of energy between the periodic dynamics of the oscillators at $E = 300\omega_m$. However, the driving amplitude at this condition is too low to

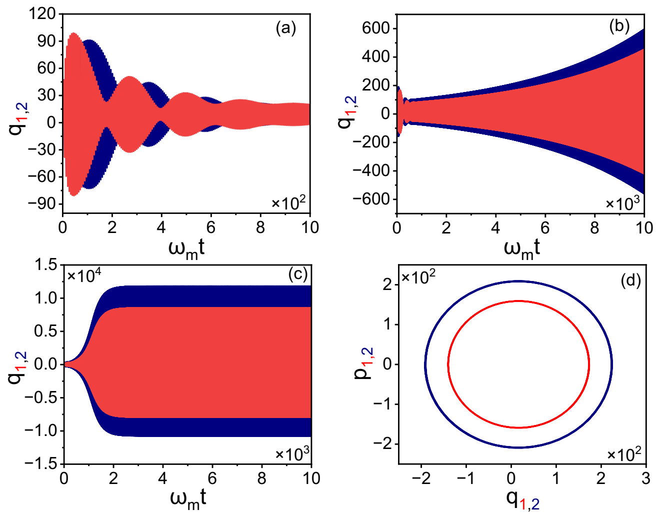

FIG. 2. (a) The classical evolution of the gain (blue) and loss (red) mechanical oscillators position $q_{1,2}$ with decaying dynamics at strong-coupling condition with driving $E = 300\omega_m$. (b) The sudden amplification in the vicinity of the exceptional point at driving $E = 400\omega_m$. (c) The self-sustained oscillation with driving $E = 500\omega_m$. (d) The corresponding phase-space trajectory at effective weak coupling.

support the energy exchange for a long time, therefore the oscillation decays. Tuning the driving amplitude towards the EP brings the system closer to the weakly coupled condition, i.e., $J < (\gamma_{\text{eff}}^1 + \gamma_{\text{eff}}^2)/4 = 0.0518\omega_m$ where the growing oscillation appears for high driving $E > E_p$. Figure 2(b) represents this condition at $E = 400\omega_m$, where the mechanical energies in both oscillators are localized, and the coupling becomes weak, therefore the energy exchange cannot be supported anymore. This localization of energy amplified the self-sustained oscillation amplitude of the oscillators. As we keep increasing E, the effective loss and gain in the oscillators cannot be balanced anymore. As a result, the gain oscillator is amplified greatly, but the loss oscillator experiences little amplification due to finite weak coupling between them. However, the optomechanical nonlinearity saturates the growth of amplification for both oscillators' amplitudes at $E = 500\omega_m$, shown in Fig. 2(c). Here we see the loss oscillator has a lesser amplitude than the gain oscillator as it continues to lose its stored mechanical energy to the environment due to a higher effective damping rate. The oscillators perform self-sustained oscillation while operating in the weak-coupling condition ($E > E_p$) and they start oscillating with a locking frequency. The phase portrait in Fig. 2(d) represents the frequency-locking phenomenon as also studied in Ref. [32]. It is important to note that, after crossing the driving amplitude threshold, there is a sudden rise in mechanical amplitude, which induces instability in the system. But the growing amplification settles as we keep on increasing the driving amplitude, eventually reaching limit cycles. This self-sustained oscillation obtained through exceptional points generates the quantum-mechanical correlations between the coupled mechanical oscillators, which will be discussed in the following section.

D. Stability and Lyapunov equation

To investigate the quantum correlation properties of the quadrature fluctuations we introduce the operators for the optical fields, i.e., $\delta\hat{x}_j = \frac{1}{\sqrt{2}}(\delta\hat{a}_j^\dagger + \delta\hat{a}_j)$ and $\delta\hat{y}_j = \frac{i}{\sqrt{2}}(\delta\hat{a}_j^\dagger - \delta\hat{a}_j)$, and for the noise operators $\delta\hat{x}_j^{\text{in}} = \frac{1}{\sqrt{2}}(\delta\hat{a}_j^{\text{in}\dagger} + \delta\hat{a}_j^{\text{in}})$ and $\delta\hat{y}_j^{\text{in}} = \frac{i}{\sqrt{2}}(\delta\hat{a}_j^{\text{in}\dagger} - \delta\hat{a}_j^{\text{in}})$. Therefore, the set of Eq. (4) describing fluctuations can be rewritten in compact matrix form as

$$\partial_t u = \mathcal{A}(t)u(t) + n(t). \tag{8}$$

Here $u^T = (\delta\hat{q}_1, \delta\hat{p}_1, \delta\hat{x}_1, \delta\hat{y}_1, \delta\hat{q}_2, \delta\hat{p}_2, \delta\hat{x}_2, \delta\hat{y}_2)$ is the quadrature fluctuation vector and $n^T = (0, \hat{\eta}_1, \sqrt{2\kappa}\delta\hat{x}_1^{\text{in}}, \sqrt{2\kappa}\delta\hat{y}_1^{\text{in}}, 0, \hat{\eta}_2, \sqrt{2\kappa}\delta\hat{x}_2^{\text{in}}, \sqrt{2\kappa}\delta\hat{y}_2^{\text{in}})$ is the input noise vector with the drift matrix $\mathcal{A}$ given as

$$\mathcal{A}^{8\times 8} = \begin{pmatrix} \mathcal{A}_1 & \mathcal{A}_0 \\ \mathcal{A}_0 & \mathcal{A}_2 \end{pmatrix} \tag{9}$$

with

$$\mathcal{A}_j = \begin{pmatrix} 0 & \omega_{mj} & 0 & 0 \\ -\omega_{mj} & -\gamma_{mj} & \sqrt{2}\,\text{Re}(G_j) & \sqrt{2}\,\text{Im}(G_j) \\ -\sqrt{2}\,\text{Im}(G_j) & 0 & -\kappa & -\Delta_j' \\ \sqrt{2}\,\text{Re}(G_j) & 0 & \Delta_j' & -\kappa \end{pmatrix}. \tag{10}$$

In addition, the 2×2 block matrix $\mathcal{A}_0$ is defined by the only nonzero element $\mathcal{A}_{21} = J$. Here $\Delta_j' = \Delta_j + g_0\langle q_j\rangle$ is the normalized effective detuning and $G_j = g_0\langle\hat{a}_j\rangle$ is the linearized effective optomechanical coupling strength where $\text{Re}(\cdot)$ and $\text{Im}(\cdot)$ indicate the real and imaginary parts of the complex quantity. Note that the driving field strength might possess any arbitrary phase associated with the mechanical quadratures [43], therefore a positive phase reference of the cavity field is assumed throughout the numerical analysis. Assuming this, only positive values of imaginary parts of $\langle\hat{a}_j\rangle$ are taken while solving the drift matrix $\mathcal{A}$. The stability conditions of the system are obtained by numerically solving the eigenvalues of the drift matrix $\mathcal{A}$, in which the system becomes unstable when any one of the real parts of the eigenvalues becomes positive [44]. Figure 3 shows the stable and unstable regions under the variation of driving amplitude. The loss oscillator is chosen as more dissipative than the gain oscillator (i.e., $\gamma_{\text{eff}}^1 > \gamma_{\text{eff}}^2$) owing to the stability analysis of the system, as it provides the decaying dynamics in strong coupling before reaching the parametric instability

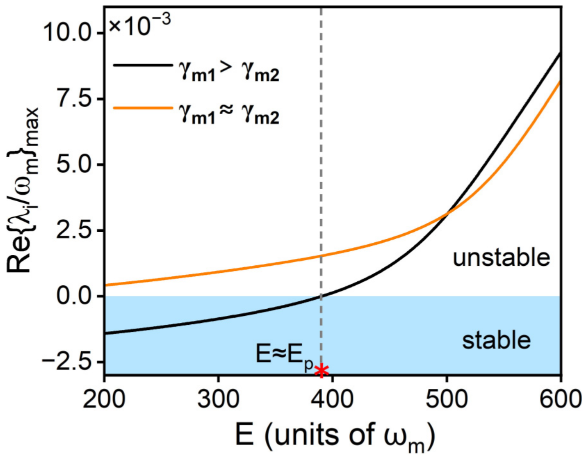

FIG. 3. The maximum eigenvalues (λ_i/ω_m) of the drift matrix $\mathcal{A}$ against the driving power for different damping ratios of the oscillators, while other parameters remain the same. The critical driving power E_p is depicted by the red star on the horizontal axis, where the system jumps from stable to unstable region.

point (EP), as indicated by Eq. (7) and shown in Fig. 2(a). Figure 3 shows that the EP matches the transition from stable to unstable region by considering the aforementioned dissipative condition. For identical damping rates, i.e., $\gamma_{\text{eff}}^1 \approx \gamma_{\text{eff}}^2$, both mechanical oscillators lead to effectively balanced gain-loss in the system, operation in that condition may induce finite oscillations before reaching the EP, and the transition from decaying dynamics to self-sustained oscillation will not be visible. The instability reached via EP essentially amplifies the mechanical amplitudes of the oscillators, leading to limit cycle oscillation, as also confirmed by imbalanced gain-loss conditions related to mechanical and optical $\mathcal{PT}$ symmetric systems [31,35]. The limit cycles reached via EP are essential to develop quantum phase synchronization and entanglement simultaneously in the proposed system.

The correlation properties of quadrature fluctuations can be found by studying the evolution of $\mathcal{A}$ and the formal solution of Eq. (8) can be expressed as $u(t) = M(t)u(0) + \int_0^t M(\tau)n(t-\tau)d\tau$, where $M(t) = e^{\mathcal{A}t}$ and n is the input noise vector. Since the fluctuation dynamics in Langevin equations are linearized and noise for both optical and mechanical systems is assumed as zero-mean Gaussian distribution, the evolved states are also time-dependent Gaussian states with zero mean irrespective of the initial conditions [45]. Therefore, Gaussian dynamics can be fully characterized by the CM formalism [46]. Let, $\mathcal{V}$ be the covariance matrix whose elements are defined as

$$\mathcal{V} = \tfrac{1}{2}\langle u_i(t)u_j(t) + u_j(t)u_i(t)\rangle. \tag{11}$$

Here u_j is the jth entry of the quadrature vector u and the evolution of the covariance matrix and its elements are governed by the following Lyapunov equation:

$$\partial_t \mathcal{V} = \mathcal{A}\mathcal{V} + \mathcal{V}\mathcal{A}^T + \mathcal{N}. \tag{12}$$

$\mathcal{N}$ is the diffusion matrix for noise, which satisfies the correlation formula $\frac{1}{2}\langle n_i(t)n_j(t') + n_j(t')n_i(t)\rangle = N_{ij}\delta(t-t')$. This is used to deduce the noise correlation vector as $\mathcal{N} = \text{Diag}[0, \gamma(2n_m+1), \kappa, \kappa, 0, \gamma(2n_m+1), \kappa, \kappa]$. The CM for the whole system has the following form:

$$\mathcal{V}^{8\times 8} = \begin{pmatrix} \mathcal{V}_{m_1} & \mathcal{V}_{m_1,a_1} & \mathcal{V}_{m_1,m_2} & \mathcal{V}_{m_1,a_2} \\ \mathcal{V}_{a_1,m_1} & \mathcal{V}_{a_1} & \mathcal{V}_{a_1,m_2} & \mathcal{V}_{a_1,a_2} \\ \mathcal{V}_{m_2,m_1} & \mathcal{V}_{m_2,a_1} & \mathcal{V}_{m_2} & \mathcal{V}_{m_2,a_2} \\ \mathcal{V}_{a_2,m_1} & \mathcal{V}_{a_2,a_1} & \mathcal{V}_{a_2,m_2} & \mathcal{V}_{a_2} \end{pmatrix}. \tag{13}$$

Here m_1 and m_2 denote the mechanical modes of the vibrating oscillators and a_1 and a_2 are the modes corresponding to optical fields. Each block of $\mathcal{V}$ represents a 2×2 square matrix. The off-diagonal elements of the matrix represent the covariance of different subsystems, while the diagonal elements refer to the variance of each system. From this matrix, we can easily calculate the correlation properties between two different subsystems. The coupled mechanical system can be easily described by extracting the submatrix $\mathcal{V}'$ from Eq. (13), which has the following form:

$$\mathcal{V}'_{4\times 4} = \begin{pmatrix} \mathcal{V}_{m_1} & \mathcal{V}_{m_1,m_2} \\ \mathcal{V}_{m_1,m_2}^T & \mathcal{V}_{m_2} \end{pmatrix}. \tag{14}$$

By singular value decomposition, it can be shown that the 2×2 symplectic matrices of Eq. (14) can be written as $\mathcal{V}_{mj} = (2n_m+1)R(\Phi)S(2r)R^T(\Phi)$ where $S(r) = \exp[r(b_j^2 - b_j^{\dagger 2})]$ is the squeezing operator for the jth mechanical mode with squeezing parameter r and $R(\Phi) = \left(\begin{smallmatrix}\cos\phi_j & -\sin\phi_j \\ \sin\phi_j & \cos\phi_j\end{smallmatrix}\right)$ is the phase rotation operator with rotation angle ϕ_j.

E. Quantum phase synchronization

Earlier, we have demonstrated that the oscillators are phase locked for limit cycles. So, the measurement of quantum phase synchronization is appropriate to verify the quantum synchronization among quadrature fluctuations of the mechanical modes. This can be evaluated by the position and momentum vector errors for the mechanical oscillators, given as $\delta\hat{q}_- = \frac{1}{\sqrt{2}}[\delta\hat{q}_1(t) - \delta\hat{q}_2(t)]$ and $\delta\hat{p}_- = \frac{1}{\sqrt{2}}[\delta\hat{p}_1(t) - \delta\hat{p}_2(t)]$. According to Mari *et al.*'s criteria [3], the quantum phase synchronization measurement is obtained by

$$S_p = \tfrac{1}{2}\langle \delta p'_-(t)^2\rangle^{-1}. \tag{15}$$

Here, $\delta p'_- = \frac{1}{\sqrt{2}}[\delta p'_1(t) - \delta p'_2(t)]$ is the phase-locking operator associated with the mechanical oscillators:

$$\begin{pmatrix} \delta p'_j(t) \\ \delta q'_j(t) \end{pmatrix} = R(\Phi)\begin{pmatrix} \delta\hat{p}_j(t) \\ \delta\hat{q}_j(t) \end{pmatrix} \tag{16}$$

where $R(\Phi)$ is the rotation matrix and the phase is defined as $\phi_j = \tan^{-1}[\langle\hat{p}_j\rangle/\langle\hat{q}_j\rangle] \in [0, 2\pi]$. In the case of quantum phase synchronization, we obtain equal quadrature variances for both oscillators, i.e., $\langle\delta q'_-(t)^2\rangle = \langle\delta p'_-(t)^2\rangle$ [20]. An analytical expression of S_p can be obtained in the form of covariance matrix elements, and it is an unbounded quantity.

F. Bipartite Gaussian entanglement

The bipartite entanglement between two Gaussian states can be estimated with logarithmic negativity as [47,48]

$$E_n = \max[0, -\log(2\upsilon^-)] \tag{17}$$

where

$$v^- = \sqrt{\frac{\Sigma - \sqrt{\Sigma^2 - 4\det(\mathcal{V}')}}{2}} \tag{18}$$

is the smallest symplectic eigenvalue of the partial transpose of the submatrix $\mathcal{V}'$ with $\Sigma = \det(\mathcal{V}_{m_1}) + \det(\mathcal{V}_{m_2}) - 2\det(\mathcal{V}_{m_1,m_2})$. According to Simon's criterion of positive partial transpose [49], the necessary and sufficient condition for bipartite Gaussian states to be entangled is $v^- < 0.5$.

III. RESULTS AND DISCUSSION

In this section, we analyze the significance of exceptional point-induced limit cycles to establish the phenomena of quantum phase synchronization and entanglement generation between the coupled mechanical oscillators. We also represent how the shape of the Wigner function changes when we shift from strong- to weak-coupling zones, and by quantifying fidelity we establish a connection between the EP and the diverse dynamics observed in synchronization and entanglement. The impact of frequency deviations of the oscillators and decoherence due to thermal phonons is discussed finally in this section.

A. Phase synchronization and entanglement dynamics

The numerical analysis is started by solving Eq. (12), which describes the behavior of the CM elements associated with the optical and mechanical modes with initial condition $\mathcal{V}(0) = \frac{1}{2}\text{Diag}[1, 1, 1, 1, 1, 1, 1, 1]$. This corresponds to the vacuum state for both the cavities and thermal state for the mechanical oscillators with mean thermal phonon number $n_m = 0$, which can be achieved by precooling them to their ground state [50]. The CM specifies how quadrature fluctuations are correlated across different bipartite subsystems, and its elements are specified in Eq. (13). From the matrix $\mathcal{V}$, we have extracted $\mathcal{V}'$ as given in Eq. (14), which only contains information about the vibrating oscillators. $\mathcal{V}'$ is associated with the characterization of phase synchronization and entanglement parameters defined in Eqs. (15) and (17).

While tuning the driving amplitude E and surpassing the exceptional point threshold ($E > E_p$), the coupled oscillators enter into the limit cycle regime, where consistent correlations of the quadrature fluctuations are noticeable in this system. As mentioned earlier, beyond the EP there is a sudden surge in mechanical vibrations, triggering instability. Although the EP occurs at critical driving $E_p \approx 380\omega_m$, quantum correlation does not prevail until $E \approx 480\omega_m$, which is in congruence with Ref. [35]. Figure 3(a) shows phase synchronization dynamics for driving amplitudes in the self-sustained oscillation regime, and Fig. 3(b) depicts the corresponding inset. Though phase synchronization parameter S_p fluctuates at the transient stage starting from 1, it converges to a steady state asymptotically. A similar behavior is observed for entanglement dynamics E_n as shown in Fig. 3(c) with the inset in Fig. 3(d) for the same driving amplitudes as considered for the synchronization. We see the enhancement in S_p and E_n occurs with higher E as long as the driving power compensates for the weak effective coupling condition. However, the phase synchronization parameter increases dramatically with E in comparison with logarithmic negativity. We also notice the death and rebirth of entanglement [51] happens at the low driving strength $E = 500\omega_m$, which is closer to the EP and vanishes quickly as the optical power increases. The dynamics can be controlled with driving amplitude (E) and various frequency mismatches ($\delta\omega_m$) between the oscillators, which is discussed later in this section. Over time, entanglement and synchronization both exhibit periodic variations because quantum fluctuations follow classical periodic orbits as long as all Lyapunov exponents of the classical equations are negative [52]. It is essential to understand that steady quantum correlation dynamics arise with weak-coupling conditions only. When the driving amplitude is not strong enough ($E < E_p$), classical dynamics decays, and the oscillators do not entangle or synchronize.

B. Wigner's distribution and fidelity

To further confirm the influence of the exceptional point on synchronization and entanglement, we plot the two-mode Wigner distribution function $W(q, p)$ of the coupled oscillators for various optical driving amplitudes. The Gaussian Wigner distribution of the two mechanical modes m_1 and m_2 is defined as [53,54]

$$W(q, p) = \frac{1}{2\pi\sqrt{\det(\mathcal{V}_{m_j})}} \exp\left[-\frac{u_j \mathcal{V}_{m_j}^{-1} u_j^T}{2}\right] \tag{19}$$

where $j = 1, 2$ represents the two coupled oscillators and u_j and $\mathcal{V}_{mj}$ are first- and second-order moment vectors of the jth mechanical mode. The first-order moment vector, u_j, indicates the position of the origin and the second-moment vector $\mathcal{V}_{mj}$ can be found from diagonal block matrices of Eq. (14). However, u_j does not provide any relevant information and can be conveniently set to zero. The phase-space distribution of the gain (loss) oscillators is represented with blue (red) colors in Fig. 5 with the variation of E. When the driving amplitude is low, such as $E = 200\omega_m$, it corresponds to both oscillators being in their ground state with nearly equal distribution function (W) and identical Gaussian states. This occurs because of the strong coupling, which causes a coherent exchange of energy between them. Increasing E to $300\omega_m$ causes the dispersion in phase space indicating a lower Wigner density function. This fact can also be verified by the decaying dynamics of classical oscillation in Fig. 2(a). Near the exceptional point at $E = 400\omega_m$, we notice an overlapping in the Wigner distribution functions, and the two mechanical modes are closest at that time. The Wigner distributions are almost indistinguishable until this driving amplitude limit. Further increasing E causes the mechanical amplification after the EP and the Wigner functions become delocalized with abrupt stretching occurring in phase space, which is a sign of dynamical instability [50]. But this delocalization vanishes quickly as the system moves away from the exceptional point and reaches limit cycles for $E = 500\omega_m$. The squeezing effect is visible among the oscillators for limit cycle driving power, depicted in the lower panel of Fig. 5. Although there are certain periods with $E_n = 0$ in the temporal evolution of entanglement due to the lower optical drive in Fig. 4(d), this is not reflected in the squeezing characteristics of Fig. 5. As long

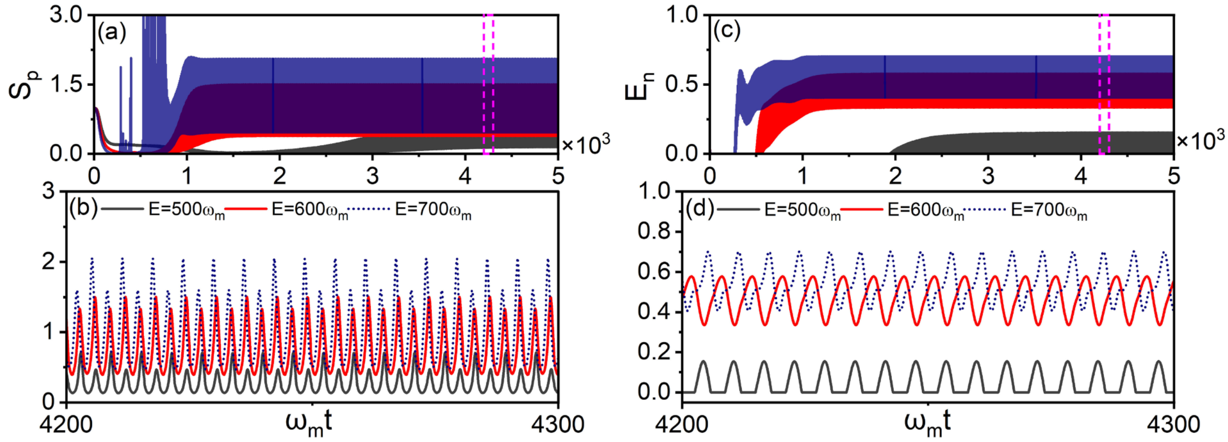

FIG. 4. (a), (c) The time evolution of quantum phase synchronization and logarithmic negativity at different optical driving strengths in the limit cycle regime. (b), (d) The magnified plot for the time duration $\omega_m t = 4200 \rightarrow 4300$ (marked by two vertical dotted lines) with $E = 500\omega_m$ (black), $E = 600\omega_m$ (red), and $E = 700\omega_m$ (blue) for $n_m = 0$. The other parameters remain the same.

as the Wigner function remains localized in phase space with finite squeezing and no abrupt stretching, we can ensure there is a certain amount of quantum correlations (such as entanglement) present between the Gaussian states. In other words, the onset of entanglement between the coupled mechanical oscillators is guaranteed by the squeezed behavior of the phase-space distributions. Additionally, the Wigner density functions start rotating in phase space. Similar to the classical case as discussed earlier, the weak-coupling condition is also exhibited in the Wigner distribution. As E further increases beyond the EP, the degree of phase-space rotation as well as the squeezing magnitude of the oscillators change. The origin of phase synchronization and entanglement dynamics in the limit cycle regime driving amplitudes in Fig. 4 can be

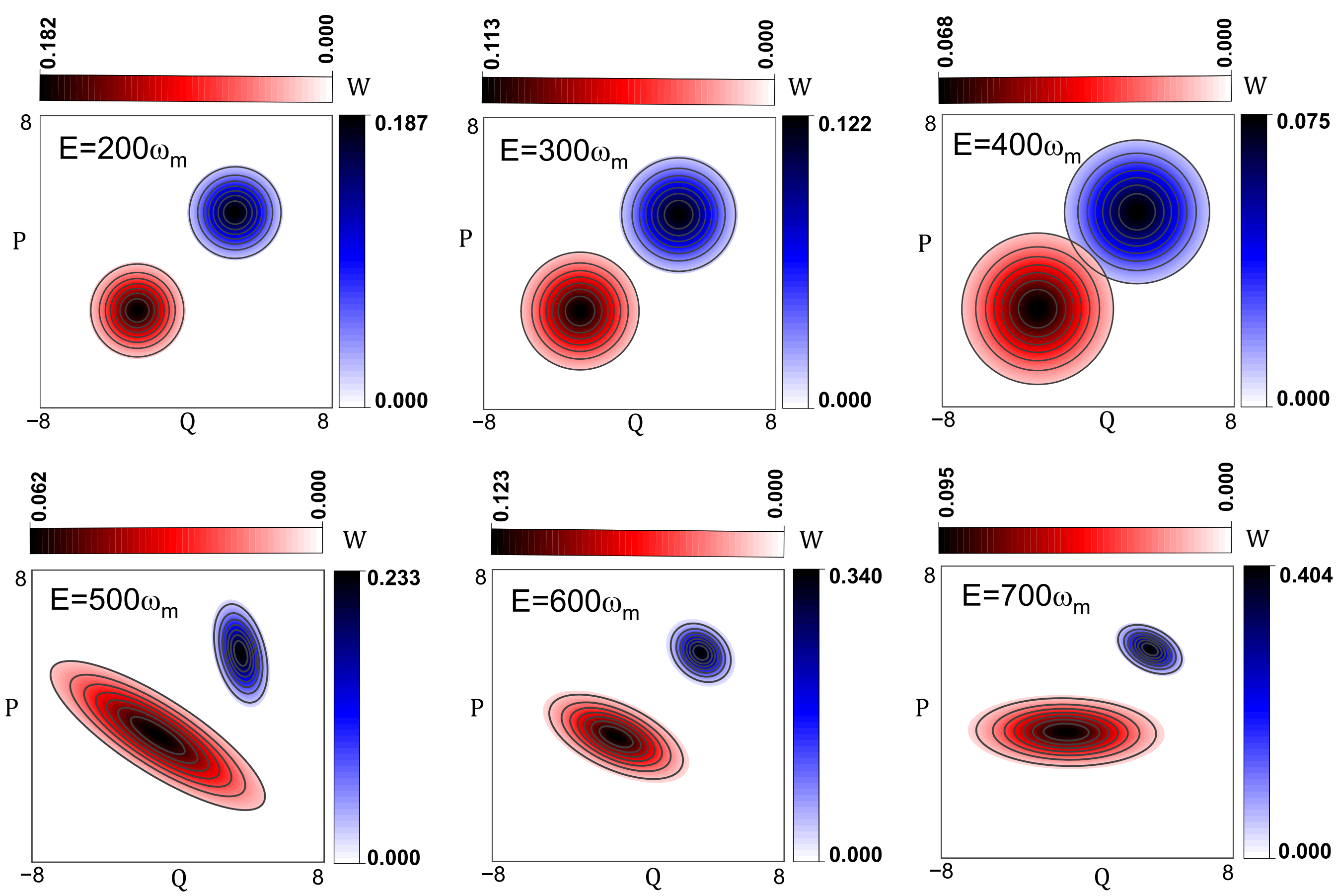

FIG. 5. The Wigner function visualization of the coupled gain (blue) and loss (red) mechanical system. The upper panel represents the distribution functions of the unsqueezed states, while the lower panel represents the squeezed states by varying the optical driving strength.

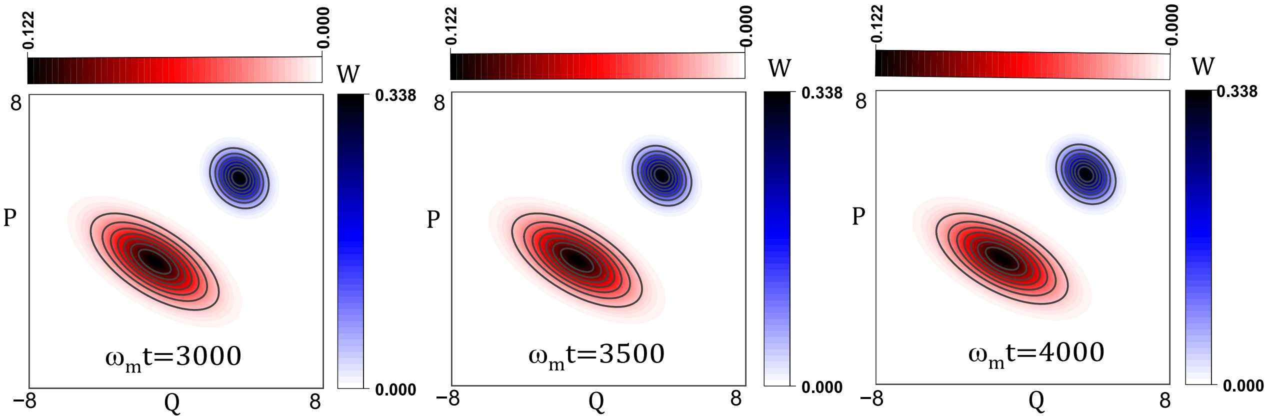

FIG. 6. The time evolution of the gain (blue) and loss (red) Wigner density functions at time instants $\omega_m t = 3000$, $\omega_m t = 3500$, and $\omega_m t = 4000$ at fixed power $E = 600\omega_m$.

traced back to this point. Also, the shape and angle of rotation of Wigner functions remain constant over time, at a fixed driving amplitude. Figure 6 represents W at three subsequent time intervals with optical driving $E = 600\omega_m$. Note that the two coupled oscillators are phase synchronized with the same magnitude of squeezing, indicating persistent entanglement. Therefore, we ensure the proposed system exhibits both phase synchronization and entanglement simultaneously.

Another important method to verify the geometry of Wigner functions is by calculating fidelity for the Gaussian states. In this system, fidelity is determined by comparing the overlap of two Gaussian states. Essentially, it measures the level of similarity between these states, defined as [53,54]

$$F = \frac{\exp\left[-\frac{1}{2}(u_1 - u_2)(\mathcal{V}_{m_1} + \mathcal{V}_{m_1})^{-1}(u_1 - u_2)^T\right]}{\sqrt{\delta_1 + \delta_2} - \sqrt{\delta_2}} \tag{20}$$

with $\delta_1 = \det(\mathcal{V}_{m_1} + \mathcal{V}_{m_1})$ and $\delta_2 = 4(\det[\mathcal{V}_{m_1}] - 0.25)(\det[\mathcal{V}_{m_2}] - 0.25)$. The behavior of fidelity (F) dynamics is illustrated in Fig. 7 under varying optical powers. Initiated at $F = 1$ during the transient stage, fidelity

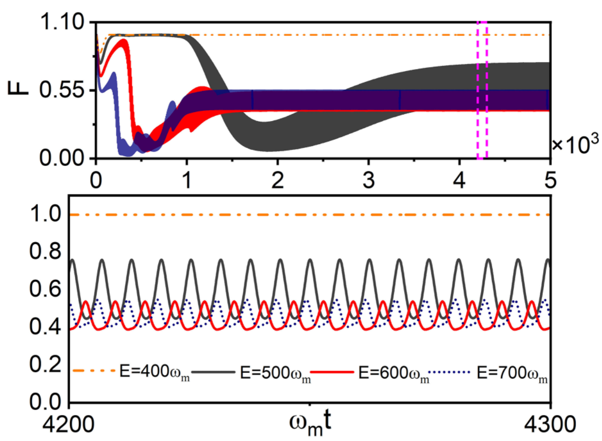

FIG. 7. The evolution of the fidelity dynamics at driving strength $E = 400\omega_m$ (orange), $E = 500\omega_m$ (black), $E = 600\omega_m$ (red), and $E = 700\omega_m$ with the magnified plot for the time duration $\omega_m t = 4200 \rightarrow 4300$ shown in the lower panel. The dynamics are plotted by considering thermal phonons $n_m = 0$.

subsequently diminishes in the steady state for limit cycles. As anticipated from the Wigner distribution functions depicted in Fig. 5, fidelity remains at unity near the exceptional point, i.e., $E = 400\omega_m$, exhibiting no fluctuations as represented by the orange dotted line in the inset image. Moving away from the exceptional point, fidelity experiences a decline, as evident by the distinct shapes of the squeezed Wigner distributions. Figure 7 portrays diverse fidelity dynamics within the limit cycle regime, employing driving amplitude levels consistent with those taken previously. We see that fidelity represented with the black curve ($E = 500\omega_m$) is higher than the red ($E = 600\omega_m$) and blue ($E = 700\omega_m$) curve, which depicts opposite behavior than phase synchronization and entanglement dynamics. The fidelity fluctuation persists in the limit cycle oscillation of the mechanical oscillators. As one can observe from Fig. 5, the Gaussian states represented by the Wigner distribution are almost identical for $E \lesssim 400\omega_m$, therefore $F = 1$ is imperative. In this scenario, no quantum correlations are observed, but the indistinguishable nature is lost when mechanical squeezing modifies the Gaussian states for $E \gtrsim 500\omega_m$, due to which fidelity dynamics start to fluctuate below $F = 1$. The fluctuation of fidelity indicates a greater likelihood of synchronization and entanglement [55], which was also verified in Fig. 4.

C. Effect of frequency mismatch and finite thermal phonons

The frequency mismatch of the coupled mechanical oscillators plays a crucial role in examining the phase synchronization and entanglement characteristics. To explore the influence of frequency deviations, we varied the frequency mismatch, i.e., $\delta\omega_m = \omega_{m2} - \omega_{m1}$ till $0.01\delta\omega_m$ while tuning the driving amplitude E in the limit cycle regime. Note that $\delta\omega_m$ should remain small due to the assumption considered in the classical analysis. Figure 8 represents the effect of $\delta\omega_m$ on quantum phase synchronization and logarithmic negativity, showing different zones of maximum and minimum values of S_p and E_n. From Fig. 8(a) it can be observed for lower mismatch, i.e., $\delta\omega_m < 0.002$, that a smaller range of optical driving ($E \gtrsim 700\omega_m$) is sufficient to synchronize the oscillators, while with a higher mismatch, i.e., $\delta\omega_m > 0.005$, a wider range of E is required in the limit cycle regime.

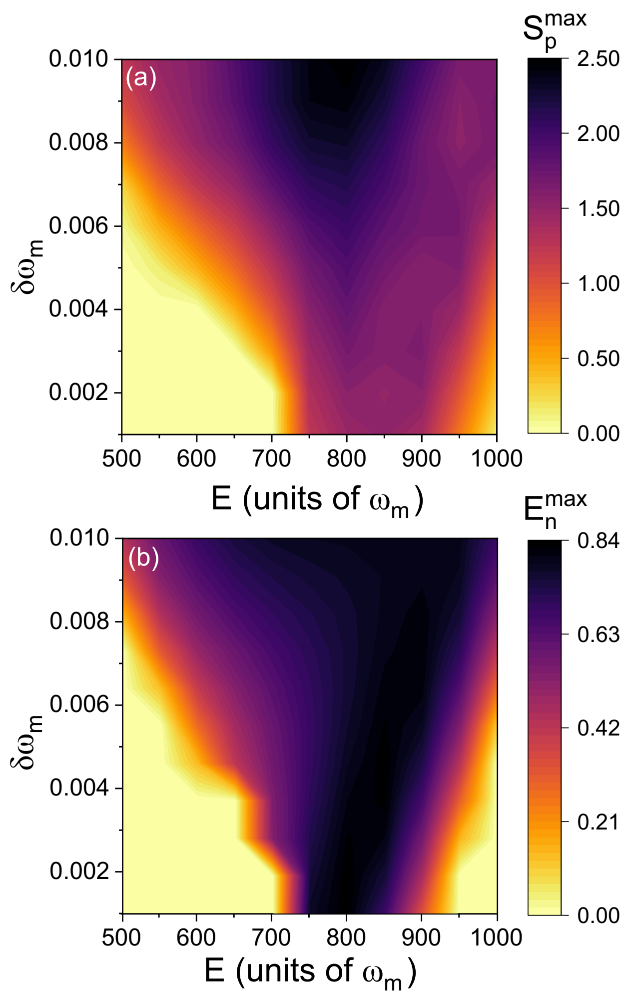

FIG. 8. (a) The maximum of the quantum phase synchronization and (b) the entanglement with the varying frequency mismatch ($\delta\omega_m$) and the optical driving power (E) in the self-sustained oscillation regime.

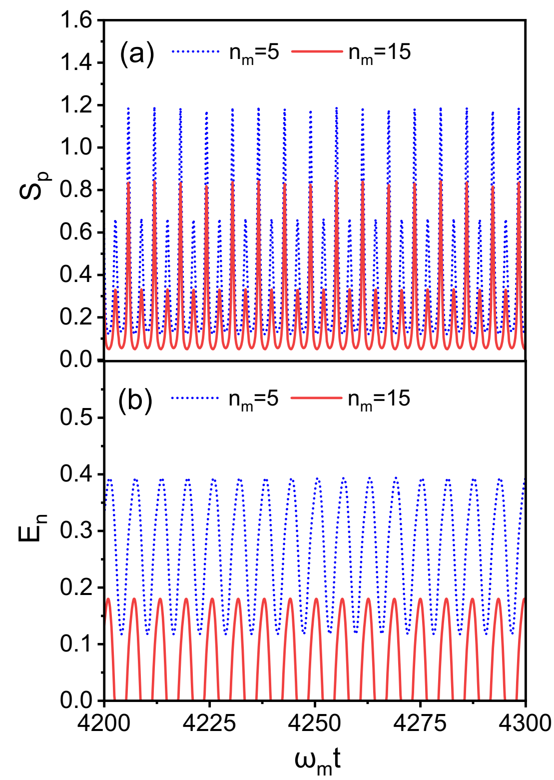

FIG. 9. The time evolution of (a) the quantum phase synchronization and (b) the entanglement for a finite thermal phonon number of $n_m = 5$ (blue) and $n_m = 15$ (red) with the driving power amplitude fixed at $E = 600\omega_m$.

$S_p^{\max}$ occurs in between $E = 700\omega_m$ and $900\omega_m$ with frequency deviation ranging from 0.007 to 0.01. For this reason, we have fixed $\delta\omega_m = 0.008$ in the earlier numerical simulations. Interestingly, we observe a stronger tendency towards phase synchronization with an increase in $\delta\omega_m$, which is contradictory to the classical case, yet similar to the blockade phenomenon [56]. However, the physical mechanism of quantum synchronization blockade is different in this case, which depends upon the simultaneous cooling of the mechanical modes as discussed in Ref. [23]. We also notice a similarity of quantum phase synchronization with entanglement in Fig. 8, which further establishes their simultaneous generation and control. However, the occurrence of $E_n^{\max}$ does not depend upon $\delta\omega_m$, unlike $S_p^{\max}$. We see that maximum logarithmic negativity values can be obtained from lower- to higher-frequency deviations and they fall in the driving power range of $750\omega_m \lesssim E \lesssim 950\omega_m$. Therefore, we expect that a moderate frequency deviation of the mechanical oscillators does not affect much the quantum phase synchronization and entanglement formation.

Lastly, it is important to discuss the impact of thermal phonons on quantum dynamics to analyze the deviations. The calculations mentioned so far do not account for thermal noise. However, as the system temperature rises, there is a corresponding increase in mean thermal phonon numbers. Figure 9 displays dynamics of phase synchronization and entanglement for different thermal phonon numbers when increased from an idealistic condition of $n_m = 0$ to $n_m = 5$ and 15. As the temperature increases, entanglement and phase synchronization dynamics diminish, due to the decoherence. However, phase synchronization is more resilient than entanglement, even at high temperatures.

IV. CONCLUSION

In this paper, we explored entanglement and quantum phase synchronization dynamics in a gain-loss optomechanical system with mechanically coupled oscillators. By applying opposite detunings, we induced gain and loss effects in the mechanical oscillators and controlled various dynamics both classically and quantum mechanically by varying the optical driving amplitude. Using experimentally feasible parameters, we observed various oscillation dynamics, including damping and self-sustained vibrations. These oscillators showed phase-locked behavior in the weak-coupling condition resulting in limit cycles, which could be accessed by adjusting laser power and tuning the exceptional point. Quantum correlations of quadrature fluctuation operators emerged during limit

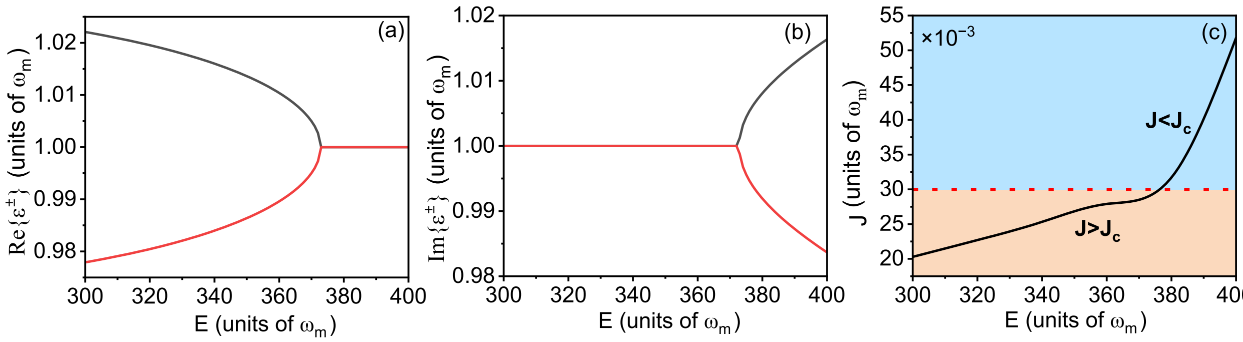

FIG. 10. The real (a) and imaginary parts (b) of the eigenvalues. The EP occurs in the parameter space for the critical coupling strength J_c with corresponding driving amplitude $E = E_p$, and other parameters are taken the same as before. (c) The variation of critical coupling strength where driving amplitude below the red dotted line indicates effective strong coupling and that above it represents effective weak-coupling regions.

cycle oscillations, revealing entanglement and synchronized quantum phases between the coupled mechanical modes. As driving amplitude is increased, the effective coupling becomes weaker, and entanglement and synchronization dynamics are enhanced. These phenomena initially grew but later decreased due to factors like higher driving strength and various frequency mismatches. Corresponding Wigner function distributions help to visualize the evolved Gaussian states that are squeezed and phase-space rotated. Also, the fidelity dynamics is calculated to verify how different geometries of the Wigner function are related to fidelity fluctuation, which in turn controls phase synchronization and entanglement dynamics. Remarkably, phase synchronization remained robust against finite thermal noise compared to entanglement, which is more sensitive to temperature changes. From an engineering point of view, a perfectly balanced condition is not always practically realizable, and moderate frequency deviation of the mechanical oscillators does not affect much our system. The numerical calculations show that mechanical oscillators can be used to manipulate Gaussian quantum information through the phonon transfer mechanism that acts as Gaussian channels.

APPENDIX: EXCEPTIONAL POINT ANALYSIS

The growth of mechanical amplitudes is slow over time in the limit cycle oscillations, thus the cavity modes $\langle\hat{a}_j\rangle$ can be safely eliminated from Eq. (5) by assuming a fixed amplitude for the mechanical vibrations. With this assumption, the set of Eq. (5) can be solved by describing the mechanical oscillation with the aforementioned ansatz formula as [32]

$$\langle\hat{b}_j\rangle = \beta_j^{\mathrm{SS}} + \tilde{\beta}_j \exp(-i\bar{\omega}_m t) \tag{A1}$$

where $\beta_j^{\mathrm{SS}} = \frac{ig_0|\langle\hat{a}_j\rangle|^2 + iJ\beta_{3-j}^{\mathrm{SS}}}{i\omega_{mj}+\gamma_{mj}}$ [obtained by setting $\partial_t\langle\hat{b}_j\rangle = 0$ in Eq. (5)], and by using the Jacobi-Anger expansion the intracavity field can be expressed as

$$\langle\hat{a}_j\rangle = \exp(-i\theta_j)\sum_n \alpha_j^n \exp(in\bar{\omega}_m t) \tag{A2}$$

where $\theta_j = -\nu_j \sin\bar{\omega}_m t$ is the phase with $\nu_j = \frac{2g_0\,\mathrm{Re}(\tilde{\beta}_j)}{\bar{\omega}_m}$ and the different harmonics of the cavity field are

$$\alpha_j^n = \frac{EJ_n(-\nu_j)}{\kappa + i(n\omega_m - \Delta'_j)}. \tag{A3}$$

Here J_n is the nth-order Bessel function of the first kind where $i(n\omega_m - \Delta'_j) + \kappa$ can be expressed as l_n^j and $\Delta'_j = \Delta_j + 2g_0\,\mathrm{Re}(\beta_j^{\mathrm{SS}})$. Substituting the expressions into Eq. (5), we get the coupled mechanical modes without the cavity fields as [40]

$$\begin{aligned}\partial_t\langle\hat{b}_1\rangle &= -\left(i\omega_{\mathrm{eff}}^1 + \gamma_{\mathrm{eff}}^1\right)\langle\hat{b}_1\rangle + iJ\langle\hat{b}_2\rangle,\\ \partial_t\langle\hat{b}_2\rangle &= -\left(i\omega_{\mathrm{eff}}^1 - \gamma_{\mathrm{eff}}^1\right)\langle\hat{b}_2\rangle + iJ\langle\hat{b}_1\rangle.\end{aligned} \tag{A4}$$

The optomechanical modifications for effective frequency and effective damping rates while eliminating the cavity fields are expressed as $\omega_{\mathrm{eff}}^j = \omega_{mj} + \omega'_j$ and $\gamma_{\mathrm{eff}}^j = \gamma_{\mathrm{opt}}^j \pm \gamma_{mj}$ [31]. Here, ω'_j is known as the optical spring effect and γ_{opt}^j is the optomechanically modified damping rate, which is given as [32]

$$\begin{aligned}\omega'_j &= -\frac{2g_0^2E^2}{\Omega\nu_j}\,\mathrm{Re}\sum_n \frac{J_{n+1}(-\nu_j)J_n(-\nu_j)}{l_{n+1}^{j*}l_n^j},\\ \gamma_{\mathrm{opt}}^j &= \frac{4\kappa g_0^2E^2}{\nu_j}\sum_n \frac{J_{n+1}(-\nu_j)J_n(-\nu_j)}{\left|l_{n+1}^{j*}l_n^j\right|^2}.\end{aligned} \tag{A5}$$

In the limit of conservative systems, the Bessel functions can be approximated as

$$\begin{aligned}J_n(-\nu) &\approx \frac{1}{n!}\left(\frac{-\nu}{2}\right)^n, \quad \text{for} \quad n > 0,\\ J_n(-\nu) &\approx \frac{(-1)^n}{(-n)!}\left(\frac{-2}{\nu}\right)^n, \quad \text{for} \quad n < 0.\end{aligned} \tag{A6}$$

Since $\nu \ll 1$ implies $\frac{-\nu}{2} \sim 0$ for $n \gg 1$, we take $n = -1, 0$, that yields [41]

$$\gamma_{\mathrm{opt}}^j \approx \frac{4g_0^2}{\kappa}|\langle\hat{a}_j\rangle^{\mathrm{SS}}|^2. \tag{A7}$$

Here $\langle\hat{a}_j\rangle^{\mathrm{SS}}$ is the steady-state amplitude of the optical field given as $\langle\hat{a}_j\rangle^{\mathrm{SS}} = E/(\kappa - i\Delta'_j)$ [also obtained by setting $\partial_t\langle\hat{a}_j\rangle = 0$ in Eq. (5)]. These expressions are obtained in the linear regime with amplitude-independent ω_j' and γ_{opt}^j terms. By incorporating all modifications into the gain-loss system, the effective Hamiltonian of Eq. (6) is obtained with the corresponding eigenvalues given as

$$\epsilon^{\pm} \approx \frac{\omega_{m1}+\omega_{m2}}{2} - i\frac{\gamma_{\text{eff}}^1-\gamma_{\text{eff}}^2}{4} \pm \sqrt{J^2-J_c^2}. \tag{A8}$$

The eigenvalues are numerically estimated in Fig. 10 by assuming $\delta\omega_m = 0$, which is found near $372\omega_m$, and it resembles closely with the earlier analytical anlysis when finite $\delta\omega_m$ is considered. From Figs. 10(a) and 10(b) we see the splitting characteristics of eigenvalues upon reaching the exceptional point of the system. Here $J_c = \frac{\gamma_{\text{eff}}^1+\gamma_{\text{eff}}^2}{4}$ is the critical coupling strength that depends upon the effective damping rates of the mechanical oscillators. By tuning the driving amplitude (E), the EP can be adjusted to match the critical coupling strength J_c. Figure 10(c) depicts the effective strongly coupled region ($J > J_c$) for $E \lesssim E_p$ and the effective weakly coupled region ($J < J_c$) for $E \gtrsim E_p$, respectively.

[1] C. Huygens and H. M. der Wetenschappen, *Oeuvres Complètes de Christiaan Huygens* (M. Nijhoff, 1905).
[2] A. Pikovsky, M. Rosenblum, and J. Kurths, *Synchronization: A Universal Concept in Nonlinear Sciences*, Cambridge Nonlinear Science Series (Cambridge University Press, Cambridge, 2001).
[3] A. Mari, A. Farace, N. Didier, V. Giovannetti, and R. Fazio, Measures of quantum synchronization in continuous variable systems, Phys. Rev. Lett. **111**, 103605 (2013).
[4] W. Li, F. Zhang, C. Li, and H. Song, Quantum synchronization in a star-type cavity QED network, Commun. Nonlinear. Sci. Numer. Simul. **42**, 121 (2017).
[5] M. Xu, D. A. Tieri, E. C. Fine, J. K. Thompson, and M. J. Holland, Synchronization of two ensembles of atoms, Phys. Rev. Lett. **113**, 154101 (2014).
[6] T. E. Lee, C.-K. Chan, and S. Wang, Entanglement tongue and quantum synchronization of disordered oscillators, Phys. Rev. E **89**, 022913 (2014).
[7] A. Roulet and C. Bruder, Quantum synchronization and entanglement generation, Phys. Rev. Lett. **121**, 063601 (2018).
[8] V. Ameri, M. Eghbali-Arani, A. Mari, A. Farace, F. Kheirandish, V. Giovannetti, and R. Fazio, Mutual information as an order parameter for quantum synchronization, Phys. Rev. A **91**, 012301 (2015).
[9] G. L. Giorgi, F. Galve, G. Manzano, P. Colet, and R. Zambrini, Quantum correlations and mutual synchronization, Phys. Rev. A **85**, 052101 (2012).
[10] R. Quan, Y. Zhai, M. Wang, F. Hou, S. Wang, X. Xiang, T. Liu, S. Zhang, and R. Dong, Demonstration of quantum synchronization based on second-order quantum coherence of entangled photons, Sci. Rep. **6**, 30453 (2016).
[11] R. Jozsa, D. S. Abrams, J. P. Dowling, and C. P. Williams, Quantum clock synchronization based on shared prior entanglement, Phys. Rev. Lett. **85**, 2010 (2000).
[12] D. Witthaut, S. Wimberger, R. Burioni, and M. Timme, Classical synchronization indicates persistent entanglement in isolated quantum systems, Nat. Commun. **8**, 14829 (2017).
[13] M. Aspelmeyer, T. J. Kippenberg, and F. Marquardt, Cavity optomechanics, Rev. Mod. Phys. **86**, 1391 (2014).
[14] W. Li, C. Li, and H. Song, Quantum synchronization in an optomechanical system based on Lyapunov control, Phys. Rev. E **93**, 062221 (2016).
[15] S. Kalita, S. Chakraborty, and A. K. Sarma, Switching of quantum synchronization in coupled optomechanical oscillators, J. Phys. Commun. **5**, 115006 (2021).
[16] E. Amitai, N. Lörch, A. Nunnenkamp, S. Walter, and C. Bruder, Synchronization of an optomechanical system to an external drive, Phys. Rev. A **95**, 053858 (2017).
[17] L. Ying, Y.-C. Lai, and C. Grebogi, Quantum manifestation of a synchronization transition in optomechanical systems, Phys. Rev. A **90**, 053810 (2014).
[18] L. Du, C.-H. Fan, H.-X. Zhang, and J.-H. Wu, Synchronization enhancement of indirectly coupled oscillators via periodic modulation in an optomechanical system, Sci. Rep. **7**, 15834 (2017).
[19] G.-j. Qiao, H.-x. Gao, H.-d. Liu, and X. Yi, Quantum synchronization of two mechanical oscillators in coupled optomechanical systems with Kerr nonlinearity, Sci. Rep. **8**, 15614 (2018).
[20] G. J. Qiao, X. Y. Liu, H. D. Liu, C. F. Sun, and X. X. Yi, Quantum ϕ synchronization in a coupled optomechanical system with periodic modulation, Phys. Rev. A **101**, 053813 (2020).
[21] D. Garg, Manju, S. Dasgupta, and A. Biswas, Quantum synchronization and entanglement of indirectly coupled mechanical oscillators in cavity optomechanics: A numerical study, Phys. Lett. A **457**, 128557 (2023).
[22] G. Wang, L. Huang, Y.-C. Lai, and C. Grebogi, Nonlinear dynamics and quantum entanglement in optomechanical systems, Phys. Rev. Lett. **112**, 110406 (2014).
[23] C.-G. Liao, R.-X. Chen, H. Xie, M.-Y. He, and X.-M. Lin, Quantum synchronization and correlations of two mechanical resonators in a dissipative optomechanical system, Phys. Rev. A **99**, 033818 (2019).
[24] Manju, S. Dasgupta, and A. Biswas, Entanglement boosts quantum synchronization between two oscillators in an optomechanical setup, Phys. Lett. A **482**, 129039 (2023).
[25] Ş. K. Özdemir, S. Rotter, F. Nori, and L. Yang, Parity-time symmetry and exceptional points in photonics, Nat. Mater. **18**, 783 (2019).
[26] K. G. Makris, R. El-Ganainy, D. N. Christodoulides, and Z. H. Musslimani, Beam dynamics in PT symmetric optical lattices, Phys. Rev. Lett. **100**, 103904 (2008).
[27] A. Guo, G. J. Salamo, D. Duchesne, R. Morandotti, M. Volatier-Ravat, V. Aimez, G. A. Siviloglou, and D. N. Christodoulides, Observation of PT-symmetry breaking in complex optical potentials, Phys. Rev. Lett. **103**, 093902 (2009).
[28] B. Peng, Ş. K. Özdemir, F. Lei, F. Monifi, M. Gianfreda, G. L. Long, S. Fan, F. Nori, C. M. Bender, and L. Yang, Parity-time-symmetric whispering-gallery microcavities, Nat. Phys. **10**, 394 (2014).
[29] P. Djorwe, Y. Pennec, and B. Djafari-Rouhani, Exceptional point enhances sensitivity of optomechanical mass sensors, Phys. Rev. Appl. **12**, 024002 (2019).
[30] H. Lü, C. Wang, L. Yang, and H. Jing, Optomechanically induced transparency at exceptional points, Phys. Rev. Appl. **10**, 014006 (2018).

[31] S. Mondal and K. Debnath, Controllable optical-sideband generation and synchronization in a mechanical gain-loss optomechanical system, Phys. Rev. A **108**, 023517 (2023).
[32] P. Djorwe, Y. Pennec, and B. Djafari-Rouhani, Frequency locking and controllable chaos through exceptional points in optomechanics, Phys. Rev. E **98**, 032201 (2018).
[33] P. Djorwé, Y. Pennec, and B. Djafari-Rouhani, Self-organized synchronization of mechanically coupled resonators based on optomechanics gain-loss balance, Phys. Rev. B **102**, 155410 (2020).
[34] C.-L. Zhu, Y.-L. Liu, L. Yang, Y.-X. Liu, and J. Zhang, Synchronization in PT-symmetric optomechanical resonators, Photonics Research **9**, 2152 (2021).
[35] C. Tchodimou, P. Djorwe, and S. G. Nana Engo, Distant entanglement enhanced in PT-symmetric optomechanics, Phys. Rev. A **96**, 033856 (2017).
[36] S. Chakraborty and A. K. Sarma, Delayed sudden death of entanglement at exceptional points, Phys. Rev. A **100**, 063846 (2019).
[37] Z. Li, X. Li, and X. Zhong, Optomechanical entanglement affected by exceptional point in a WGM resonator system, Opt. Express **31**, 19382 (2023).
[38] C. Gardiner and P. Zoller, *Quantum Noise: A Handbook of Markovian and Non-Markovian Quantum Stochastic Methods with Applications to Quantum Optics* (Springer, New York, 2004).
[39] R. Benguria and M. Kac, Quantum Langevin equation, Phys. Rev. Lett. **46**, 1 (1981).
[40] W. Li, C. Li, and H. Song, Theoretical realization and application of parity-time-symmetric oscillators in a quantum regime, Phys. Rev. A **95**, 023827 (2017).
[41] D. P. Foulla, P. Djorwé, S. T. Kingni, and S. G. Nana Engo, Optomechanical systems close to the conservative limit, Phys. Rev. A **95**, 013831 (2017).
[42] S. Hong, R. Riedinger, I. Marinković, A. Wallucks, S. G. Hofer, R. A. Norte, M. Aspelmeyer, and S. Gröblacher, Hanbury Brown and Twiss interferometry of single phonons from an optomechanical resonator, Science **358**, 203 (2017).
[43] C. Genes, A. Mari, P. Tombesi, and D. Vitali, Robust entanglement of a micromechanical resonator with output optical fields, Phys. Rev. A **78**, 032316 (2008).
[44] E. X. DeJesus and C. Kaufman, Routh-Hurwitz criterion in the examination of eigenvalues of a system of nonlinear ordinary differential equations, Phys. Rev. A **35**, 5288 (1987).
[45] R.-X. Chen, L.-T. Shen, Z.-B. Yang, H.-Z. Wu, and S.-B. Zheng, Enhancement of entanglement in distant mechanical vibrations via modulation in a coupled optomechanical system, Phys. Rev. A **89**, 023843 (2014).
[46] S. L. Braunstein and P. van Loock, Quantum information with continuous variables, Rev. Mod. Phys. **77**, 513 (2005).
[47] G. Vidal and R. F. Werner, Computable measure of entanglement, Phys. Rev. A **65**, 032314 (2002).
[48] P. van Loock and A. Furusawa, Detecting genuine multipartite continuous-variable entanglement, Phys. Rev. A **67**, 052315 (2003).
[49] R. Simon, Peres-Horodecki separability criterion for continuous variable systems, Phys. Rev. Lett. **84**, 2726 (2000).
[50] S. Chakraborty and A. K. Sarma, Entanglement dynamics of two coupled mechanical oscillators in modulated optomechanics, Phys. Rev. A **97**, 022336 (2018).
[51] Q.-J. Tong, J.-H. An, H.-G. Luo, and C. H. Oh, Mechanism of entanglement preservation, Phys. Rev. A **81**, 052330 (2010).
[52] Q. X. Meng, Z. J. Deng, Z. Zhu, and L. Huang, Quantum signatures of transitions from stable fixed points to limit cycles in optomechanical systems, Phys. Rev. A **101**, 023838 (2020).
[53] S. Olivares, Quantum optics in the phase space: A tutorial on Gaussian states, Eur. Phys. J.: Spec. Top. **203**, 3 (2012).
[54] C. Weedbrook, S. Pirandola, R. García-Patrón, N. J. Cerf, T. C. Ralph, J. H. Shapiro, and S. Lloyd, Gaussian quantum information, Rev. Mod. Phys. **84**, 621 (2012).
[55] S. Olivares and M. G. A. Paris, Fidelity matters: The birth of entanglement in the mixing of Gaussian states, Phys. Rev. Lett. **107**, 170505 (2011).
[56] S. E. Nigg, Observing quantum synchronization blockade in circuit quantum electrodynamics, Phys. Rev. A **97**, 013811 (2018).